# NMR Study of $Li^+$ Ion Dynamics in the Perovskite $Li_{3x}La_{1/3-x}NbO_3$

**Joël Emery,[†] Odile Bohnke,*[,‡] Pierre Florian,[§] and Kloul Marzouk[†]**

*Laboratoire de Physique de l'Etat Condensé (UMR 6087 CNRS), Laboratoire des Oxydes et Fluorures (UMR 6010 CNRS), Institut de Recherche en Ingénierie Moléculaire et Matériaux Fonctionnels (FR 2575 CNRS) Université du Maine, Avenue O. Messiaen 72085 Le Mans Cedex 9, France, Centre de Recherche sur les Matériaux à Hautes Températures, CNRS 45071, Orléans Cedex 2, France*

*Received: March 16, 2005*

$^7Li$ and $^6Li$ nuclear magnetic resonance (NMR) experiments are carried out on the perovskite $Li_{3x}La_{1/3-x}NbO_3$. The results are compared to those obtained on the titanate $Li_{3x}La_{2/3-x}TiO_3$ (LLTO) in order to investigate the effect, on the lithium ion dynamics, of the total substitution of $Nb^{5+}$ for $Ti^{4+}$ in the B-site of the $ABO_3$ perovskites. The XRD patterns analysis reveals that this substitution leads to a change in the distribution of the $La^{3+}$ ions in the structure. $La^{3+}$ ions distribution is very important, in regard to ionic conductivity, because these immobile ions can be considered as obstacles for the long-range $Li^+$ motion. If compared to the titanates, the compounds of the niobate solid solution have a bigger unit cell volume, a smaller number of $La^{3+}$ ions, and a higher number of vacancies. These should favor the motion of the mobile ions into the structure. This is not experimentally observed. Therefore, the interactions between the mobile species and their environment greatly influence their mobility. $^7Li$ and $^6Li$ NMR relaxation time experiments reveal that the Li relaxation mechanism is not dominated by quadrupolar interaction. $^7Li$ NMR spectra reveal the presence of different $Li^+$ ion sites. Some $Li^+$ ions reside in an isotropic environment with no distortion, some others reside in weakly distorted environments. $T_1$, $T_{1\rho}$, and $T_2$ experiments allow us to evidence two motions of $Li^+$. As in LLTO, $T_1$ probes a fast motion of the $Li^+$ ions inside the A-cage of the perovskite structure and $T_{1\rho}$ a slow motion of these ions from A-cage to A-cage. At variance with what has been observed in LLTO, these different $Li^+$ ions can be differentiated through the spin−lattice relaxation times, $T_1$ and $T_{1\rho}$, as well as through the transverse relaxation time, $T_2$.

## Introduction

The A-site deficient $ABO_3$ perovskites containing rare earth cations and lithium have demonstrated high lithium dc conductivity. First, Belous et al.,[1] and afterward, Inaguma et al.,[2−3] reported that lanthanum lithium titanates, $Li_{3x}La_{2/3-x}TiO_3$ (or LLTO), exhibit ionic conductivity as high as $10^{-3}$ S cm$^{-1}$ at room temperature (for $x = 0.10$) with an activation energy of 0.34 eV[3]. These titanates are the fastest lithium ion-conducting crystalline solid electrolytes known at the present time. The high lithium conductivity comes from the presence of a large number of lithium and vacancies in the A-site of the structure and from the high mobility of these mobile ions in the structure.

A better understanding of the microscopic properties of the mobile ions in these perovskites is necessary to explain the high lithium dc conductivity observed. Some attempts have already been done in our laboratories by using techniques such as nuclear magnetic resonance (NMR)[4,5] and broadband dielectric spectroscopy (BDS).[6] These techniques allowed us to clearly bring to light some important features of the $Li^+$ ion dynamics in LLTO: (i) $^7Li$ and $^6Li$ NMR relaxation time experiments showed, without doubt, that the Li relaxation is not dominated by quadrupolar interaction. (ii) Two kinds of $Li^+$ ions with slightly differing environments have been evidenced. (iii) It has also been shown that the mobile ions exhibit two different motions: a fast one, probed by the longitudinal relaxation time, $T_1$, attributed to the localized motion of these ions inside the A-cage of the perovskite $ABO_3$, and a slow one, probed by the longitudinal relaxation time in the rotating frame, $T_{1\rho}$, attributed to the $Li^+$ hopping from an A-cage to a next vacant one, corresponding to the long-range motion of the mobile ions in the oxide matrix that is also probed by the dc conductivity; these different motions have also been identified by BDS. (iv) Finally, the $T_1$ vs inverse of temperature curve exhibits a particular behavior: a strong asymmetry of the curve is observed with an increase of the activation energy as temperature increases, going from 0.14 eV in the slow regime to 0.20 eV in the fast one. In accordance with the crystallographic structure of this perovskite and especially with the unequal $La^{3+}$ ions distribution in the unit cell and the tilting of $TiO_6$ octahedra,[7,8] it has been argued that the $Li^+$ ion motion changes from a two-dimensional (2D) dimension at low temperature to a three-dimensional (3D) dimension at high temperature. A slope change was also observed around 200 K in both $T_1$ and dc conductivity curves[4,9] as well as in the ac frequency response of these oxides.[10] An exhaustive review of all the papers that appeared in the literature about these titanates can be found in ref 11.

Several papers dealing with the niobates, $Li_{3x}La_{1/3-x}NbO_3$, already appeared in the literature. Belous et al.,[12−15] Kawakami et al.,[16] and Garcia-Martin et al.[17,18] investigated their dc conductivity. However, no NMR results are available. The best reported conductivity value was on the order of $4 \times 10^{-5}$ S cm$^{-1}$ at room temperature for $x \approx 0.04$, with an activation energy of 0.37 eV.[16,17] We also performed dc conductivity

* Corresponding author. E-mail: odile.bohnke@univ-lemans.fr. Telephone: 33-2-43-83-33-54. Fax: 33-2-43-83-35-06.
[†] Laboratoire de Physique de l'Etat Condensé.
[‡] Laboratoire des Oxydes et Fluorures.
[§] Centre de Recherche sur les Matériaux à Hautes Températures.

10.1021/jp051370i CCC: $30.25 
Published on Web 10/18/2005

measurements on the samples used in this study and found the same dc conductivity and the same activation energy as reported by the other authors, i.e., $1.1 \times 10^{-5}$ S cm$^{-1}$ at 26 °C and $E_a = 0.38$ eV. Despite the increase of the unit cell volume, the activation energy is higher and the dc conductivity remains 2 orders of magnitude lower than those reported in the lanthanum lithium titanates. This result clearly shows that the ionic mobility is influenced by other parameters than the unit cell volume alone.

The aim of this paper is to go further in the understanding of the $Li^+$ ion mobility in these perovskites by probing the influence of the total substitution of $Nb^{5+}$ for $Ti^{4+}$ on the microscopic motion of the $Li^+$ ions. Therefore, we investigated the properties of the lanthanum lithium niobate, $Li_{3x}La_{1/3-x}NbO_3$ (or LLNbO), with $x = 0.04$, by $^7$Li and $^6$Li NMR spectroscopy. Such a substitution leads to the lowering of the number of $La^{3+}$ ions and then to the increase of the number of vacancies in the A-sites of the oxide. We performed measurements of the spin−lattice relaxation time $T_1$ and the transverse relaxation time $T_2$, in the temperature range from 150 to 900 K, and of the spin−lattice relaxation time in the rotating frame $T_{1\rho}$, from 150 to 410 K. The results will be compared to those obtained with the titanates[4,5] and on closely related oxides, such as $Li_xLa_{1/3}Nb_{1-x}Ti_xO_3$ studied by Latie et al.[19] The crystallographic structure of this niobate will be described carefully because the motion properties of the mobile species are closely related to the structure.

## Experimental Section

$Li_{3x}La_{1/3-x}NbO_3$ samples were synthesized from stoichiometric amounts of dehydrated $La_2O_3$ (99.999% Rhône-Poulenc), $Nb_2O_5$ (99.9% Aldrich) and $Li_2CO_3$ (99.997% Aldrich) with an excess of 10 mol % of $Li_2CO_3$ to compensate the volatilization of $Li_2O$ at high temperature. The reagents were ground in a mortar, pressed into pellets, and heated in air at 850 °C for 8 h in a platinum crucible and finally fired at 1150 °C for 10 h with a heating rate of 10 °C min$^{-1}$. The calcined powder was then ground, pressed into pellets and fired two times at 1150 °C for 10 h. The heating treatments were followed by a cooling step at a rate of 10 °C min$^{-1}$. Finally, the pellets were sintered in air at 1250 °C for 6 h.

The samples were characterized, at room temperature, by X-ray powder diffraction (XRD) on a D500 Siemens diffractometer (radiation Cu Kα, $2\theta$ range from 5° to 133°, step $\Delta 2\theta = 0.04°$, time by step = 17 s). The diffraction patterns were analysed through the Rietveld method by the Fullprof program.[20]

$^7$Li NMR experiments have been performed on a Bruker Avance 300 spectrometer for temperatures from 150 to 410 K and on a Bruker ADX 300 spectrometer for temperatures from 300 to 900 K. The experimental setups were described in ref 5. The Larmor frequency for $^7$Li was $\nu_0 = 116$ MHz. Some $^6$Li NMR experiments have also been performed at room temperature only. The Larmor frequency for $^6$Li was $\nu_0 = 44$ MHz. Static $^7$Li NMR spectra were recorded by using a simple ($^{\pi}/_2$-acquisition) sequence. A saturated LiCl solution was used as an external reference. This solution was also used to set up the radio frequency power; the $^{\pi}/_2$ liquid pulse time was 4 $\mu$s, which corresponds to a radio frequency amplitude $\nu_1 = 62.5$ kHz and to a nonselective regime. DMFIT NMR software was used to perform the deconvolution of the NMR spectra.[21]

For clarity, in this part of the paper, which deals with the dynamical aspect of ionic transport, we will use two concepts. First, about the motion: the fast motion probed by the spin−lattice relaxation time, $T_1$, and the slow motion probed by both the spin−lattice relaxation time in the rotating frame, $T_{1\rho}$, and the spin−spin relaxation time, $T_2$. Second, behind these two motions, $T_1$, $T_{1\rho}$, and $T_2$ curves vs temperature exhibit two branches named "short" and "long" with $T_\alpha^s < T_\alpha^l$ where α stands for 1, 1$\rho$, or 2.

Both the inversion−recovery sequence ($\pi-\tau-{}^{\pi}/_2$-acquisition) and the saturation-pulse sequence were used to measure the spin−lattice relaxation time, $T_1$. The two methods led to the same results. For each temperature, the data were fitted to the experimental function, either eq 1 or eq 2:

$$M(\tau) = M_0\left[1 - 2\alpha \exp\left(-\frac{\tau}{T_1}\right)\right] \quad (1)$$

$$M(\tau) = M_0\left[a_1\left(1 - 2\alpha^s \exp\left(-\frac{\tau}{T_1^s}\right)\right) + b_1\left(1 - 2\alpha^l \exp\left(-\frac{\tau}{T_1^l}\right)\right)\right] \quad (2)$$

where the spin−lattice relaxation time $T_1$'s, the thermal equilibrium magnetization $M_0$, α's, and the contributions of the two components, $a_1$ and $b_1$, were considered as free parameters in a least-squares fitting procedure. The superscript "s" refers to a short relaxation time that corresponds to a fast relaxation process, and the superscript "l" refers to a long relaxation time that leads to a slow relaxation process. The α parameters were found to be around 0.5 when using the saturation sequence and around 1 when using the inversion−recovery sequence. The goodness of the fitting procedure was determined from the deviation between the experimental and the calculated magnetization vs time curves, especially in the curvature region. The experimental value of $M(\tau)$ is obtained with an integration process.

The transverse relaxation time, $T_2$, was obtained with the ($^{\pi}/_2-\tau-\pi$-acquisition) sequence between 150 and 900 K. To account for the experimental transverse magnetization, two exponential functions were necessary, with $a_2$ and $b_2$ the contributions of each component. We used the following relationship:

$$M_\perp(\tau) = M_0\left[a_2 \exp\left(-\frac{\tau}{T_2^s}\right) + b_2 \exp\left(-\frac{\tau}{T_2^l}\right)\right] \quad (3)$$

As before, "s" stands for short and "l" for long relaxation times. In the first step of the fitting, the $a_2$ and $b_2$ parameters are respectively fixed to 0.4 and 0.6, as it is expected for relaxation in quadrupolar system.[22−27] In the second step, all the parameters constraints are relaxed. This process, also used in the $T_{1\rho}$ analysis, allows us to start fitting with theoretical results known for quadrupolar spin $^3/_2$.

To obtain the longitudinal relaxation time in the rotating frame, $T_{1\rho}$, we used the sequence ($^{\pi}/_2-\tau$ (spin lock)-acquisition) with an amplitude of the lock radio frequency field $\nu_1 = 62.5$ kHz. We have to note that the $T_{1\rho}$ experiments were not performed above 410 K because the high-temperature probe is unable to withstand the power during the locking pulse. Two $T_{1\rho}$ components were needed to account for the experimental magnetization vs time curves, thus the following function was used to obtain the $T_{1\rho}$ values:

$$M(\tau) = M_0\left[a_3 \exp\left(-\frac{\tau}{T_{1\rho}^s}\right) + b_3 \exp\left(-\frac{\tau}{T_{1\rho}^l}\right)\right] \quad (4)$$

$T_{1\rho}^s$ and $T_{1\rho}^l$ refer to the short and the long relaxation times in

the rotating frame, respectively, and $a_3$ and $b_3$ to the contributions of each component.

## Results and Discussion

Because the motion properties of a mobile species are closely related to the structure, some attention has to be paid to the crystallographic structure of the herein studied niobate. As previously reported in the literature,[13−17] a single-phase solid solution with a perovskite structure is observed in the $Li_{3x}La_{1/3-x}NbO_3$ compounds of composition ranging from $x = 0$ to $x = 0.07$. For $x > 0.07$, extra and small diffraction lines, coming from the presence of a small amount of $LiNbO_3$, are observed in the powder XRD patterns. The pure phase solid solution of niobates does not extend in the same composition domain as for the titanates, $Li_{3x}La_{2/3-x}TiO_3$, for which $x$ goes from 0.06 to 0.14. Therefore, the content of lithium ions will be always smaller in the pure solid solution of niobates than in the titanates one. According to the chemical formula, in the titanate compound with the highest conductivity, $Li_{3x}La_{2/3-x}TiO_3$ with $x = 0.10$, 57% of the A-site is occupied by big and immobile ions ($La^{3+}$), 13% only by vacancies, and 30% by $Li^+$ that are off-centered in the oxygen cage. On the other hand, in the niobate compound with $x = 0.04$, only 29% of the A-site is occupied by $La^{3+}$ ions, 59% by vacancies, and 12% by $Li^+$ ions, also off-centered in the oxygen cage. Although it is well established that conductivity is directly linked to the number of charge carriers, the small number of charge carriers in the niobate cannot explain alone the difference of 2 orders of magnitude observed in the dc conductivity, i.e., $10^{-5}$ S cm$^{-1}$ for the niobates,[14,16,17] compared to $10^{-3}$ S cm$^{-1}$ for the titanates, at room temperature. Other parameters, such as the bottleneck size, the interactions between the mobile species, and its surroundings, the number and the distribution of both the vacancies and the rare earth cations in the structure can also influence the mobility of the $Li^+$ ions in these perovskites.

Figure 1 shows powder XRD patterns of $Li_{3x}La_{1/3-x}NbO_3$ for $x = 0.025$, $x = 0.040$, and $x = 0.075$ recorded at room temperature. Apart from the reflections characteristic of the perovskite structure, superstructure lines are observed (they are marked with asterisks in the upper diagram). These superstructure lines are generally considered to originate from the ordering of $La^{3+}$ and vacancies in the A-sites, as it has been observed in the titanate $Li_{3x}La_{2/3-x}TiO_3$[7,8] and in the niobate $La_{0.33}NbO_3$.[19] At room temperature, all the patterns were indexed in a primitive orthorhombic cell deriving from that of the cubic perovskite $ABO_3$ with $a \approx a_p$, $b \approx a_p$, and $c \approx 2a_p$. Figure 2a shows the cell parameters evolution with respect to $x$. All the parameters decrease as $x$ increases, confirming that $Li^+$ ions have been incorporated into the oxide. The volume of the unit cell varies from 121.02 (± 0.01) Å$^3$ for $x = 0.01$ to 118.94 (± 0.03) Å$^3$ for $x = 0.07$. These values are slightly higher than those of LLTO, which vary from 116.52 Å$^3$ for $x = 0.06$ to 115.92 Å$^3$ for $x = 0.13$.[8] Therefore, the total substitution of $Nb^{5+}$ for $Ti^{4+}$ leads to the increase of the unit cell volume. This should facilitate the motion of the mobile ions through the oxide matrix.

The Rietveld refinement of the XRD patterns (based on the space group *Pmmm*, no. 47), clearly revealed that $La^{3+}$ ions are not randomly distributed in the A-sites of the structure. Furthermore, the refinement showed that the decrease of the intensity of the superstructure lines (Figure 1), especially the decrease of the (001) diffraction line at $2\theta = 12°$ as $x$ increases, cannot be attributed to a change in the distribution of the $La^{3+}$ ions among the 1a and 1c sites of the structure, as is the case for the titanates. This decrease is attributed, without doubt, to

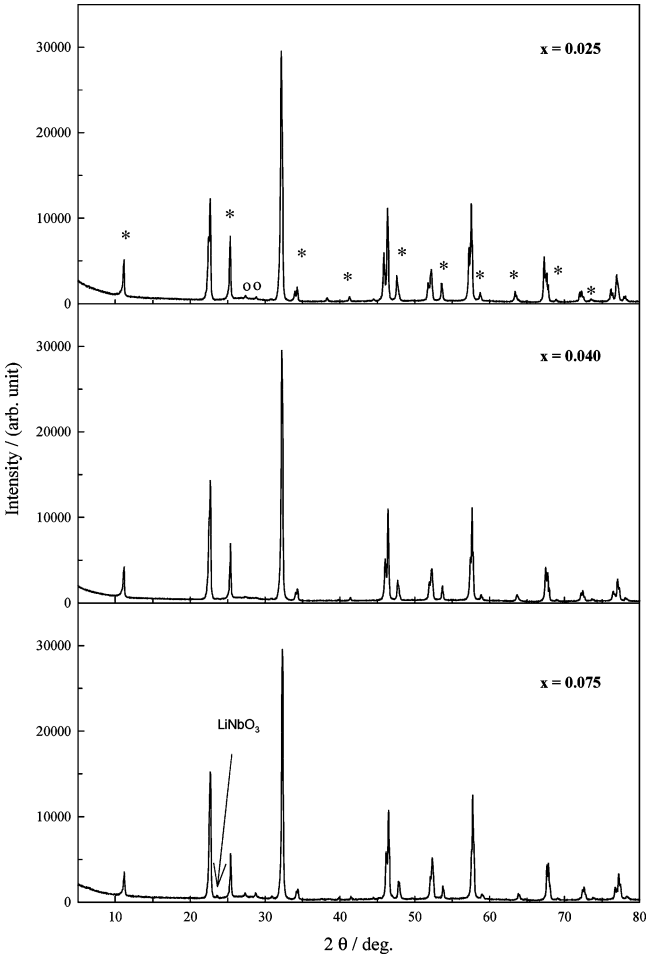


**Figure 1.** Powder X-ray diffraction patterns of $Li_{3x}La_{1/3-x}NbO_3$ samples recorded at room temperature ((○) = $LaNbO_4$, (∗) = superstructure lines).

the decrease of the $La^{3+}$ content in the material. $La^{3+}$ ions are only present in the 1a (0,0,0) site of the structure, which is occupied between 50% and 60% by $La^{3+}$ ions, depending on the composition parameter $x$, as shown in Figure 2b. On the other hand, the site 1c (0,0,$^1/_2$) is only occupied from 1% to 2.5% by $La^{3+}$ ions, which stands in the error value. This leads to the presence of two layers: a layer that contains $La^{3+}$ ions (from 50 to 60% of this layer is occupied by $La^{3+}$ ions), and a layer that does not contain any $La^{3+}$ ions. This result is at variance with what has been previously reported in the literature for the niobates.[15,16] We recall that, in the titanate, the two perovskite subcells contain $La^{3+}$ and form two layers. One layer is occupied at ≈ 90% by $La^{3+}$ ions (and forms the $La^{3+}$-rich layer), and the other one is occupied at ≈ 30% by these ions (and forms the $La^{3+}$-poor layer).[7] Furthermore, the $TiO_6$ octahedra are slightly tilted.[8] In the niobate, $La^{3+}$ ions are present in only one subcell, the number of $La^{3+}$ ions is smaller (i.e., $^1/_3 - x$), and the number of vacancies is higher (i.e., $^2/_3 - 2x$) than that in the titanate. Owing to the $La^{3+}$ distribution, a small tilting of the $NbO_6$ octahedra can also be assumed. These points are important differences in the crystal structure of the niobate if compared to the titanate one. These differences may explain some change in the mechanism of conduction. Because $La^{3+}$ ions are immobile and can be considered as obstacles for the $Li^+$ motion, the presence of a small number of $La^{3+}$ would then favor the motion of the mobile ions.

From the above results, the substitution of $Nb^{5+}$ for $Ti^{4+}$ in the perovskite leads to the increase of the unit cell and to the decrease of the number of $La^{3+}$ ions in the compounds. From

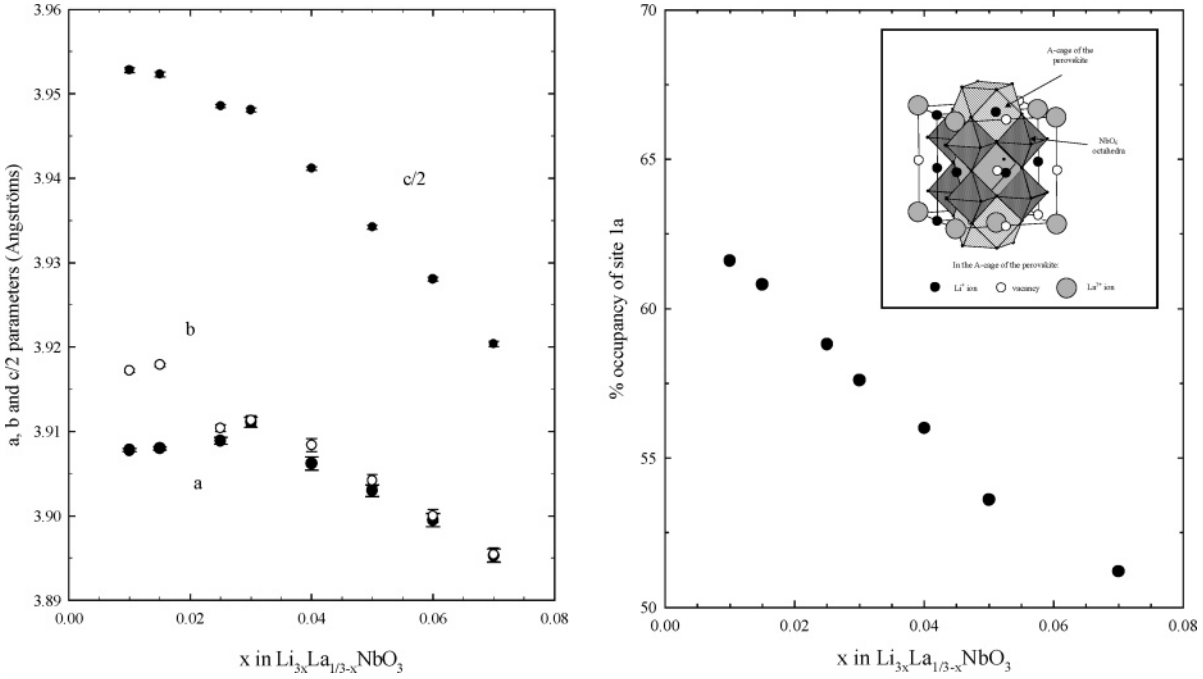


**Figure 2.** (a) Evolution of the unit cell parameters vs composition *x*. (b) La occupancy vs composition *x* for site 1a (0,0,0). The insert displays the structural model *Pmmm* (no. 47).

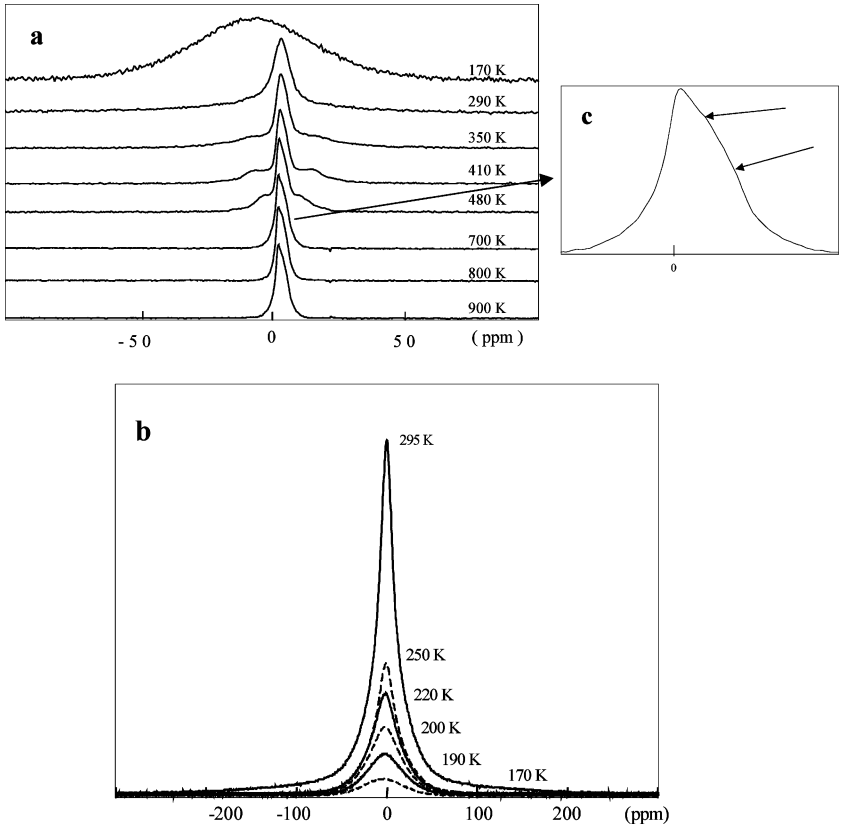


**Figure 3.** (a) Evolution of the non-normalized $^7Li$ NMR spectra as a function of temperature from 900 to 170 K. (b) Evolution of the normalized $^7Li$ NMR spectra as a function of temperature, below RT. (c) Enlarged view of the 700 K spectrum.

a structural point of view, these would lead to an increase of the mobility of the lithium ions. However, this is not experimentally observed, and then the interactions between the mobile species and their environment are important factors that certainly influence the mobility. NMR experiments may help to understand the origin of these interactions.

**$^7$Li NMR Spectra.** Figure 3a presents $^7Li$ NMR static spectra of $Li_{3x}La_{1/3-x}NbO_3$ ($x = 0.04$) recorded in the temperature range from 170 to 900 K. Owing to the large temperature range investigated, all the spectra were recorded with a static sample (without magic angle spinning) in order to keep a coherence in the results. For clarity, these spectra have not been normalized. Figure 3b shows the normalized spectra recorded below room temperature. From this set of spectra, it can be observed that both the central line and the satellites are very sensitive to the temperature. The spectra recorded between 350 and 500 K

(Figure 3a) display the typical shape of a $I = {}^3/_2$ nucleus spin with a central line coming from the transition $-{}^1/_2 \leftrightarrow +{}^1/_2$ and two satellite lines coming from the transitions $-{}^1/_2 \leftrightarrow -{}^3/_2$ and $+{}^1/_2 \leftrightarrow +{}^3/_2$ . The positions of the satellite transitions are dependent on the quadrupolar parameter, $\nu_Q$, and on the orientation of the crystallites in the static magnetic field.

At high temperature ($T \geq 700$ K, Figure 3a), the fast motion of the Li nucleus averages both the dipolar interaction (the central line narrows) and the quadrupolar interaction ($\nu_Q$ decreases). The short value of $\nu_Q$ leads to spectra that do not exhibit any quadrupolar structure. However, as shown in Figure 3c that presents an enlarged view of the 700 K spectrum, we can observe that the spectra are not symmetric, suggesting the existence of several different $Li^+$ sites in the structure (see below). As temperature decreases below 700 K, the satellite transitions appear on the spectrum, owing to the slowing down of the Li nucleus motion, which becomes not fast enough to average the quadrupolar splitting. Below 350 K (Figure 3a and b), both the central line and the satellites broaden. Consequently, the satellite transitions disappear again. The central line broadening is essentially due to the dipolar interaction because it is well-known that, for a nucleus whose spin is half integer, the central line is not sensitive to the quadrupolar interaction (first order of perturbations). The appearance of the quadrupolar structure, when temperature increases, arises from the averaging of the dipolar interaction before the motion averages the quadrupolar interaction. Such a result has been already observed in LLTO.[4]

The analysis of these spectra is particularly difficult for several reasons. First, we are concerned with a powder made of different crystallites. Each crystallite has its own orientation in the magnetic field and, consequently, its own splitting of its satellite transitions. Second, as suggested previously, several $Li^+$ sites with different environments (and different $\nu_Q$) and/or some $Li^+$ disorder (with a continuous distribution of sites and then of $\nu_Q$) may exist in the structure. This also would lead to different splitting of the satellite transitions. Third, the motional averaging, which appears when the frequency of the motion is larger than the splitting of the satellite transitions, may act differently on the different points of the spectrum, especially in the intermediate regime. Finally, it is possible that the central transition does not behave exactly as the satellite ones. According to these above considerations, it becomes difficult to follow the different spectrum parameters as a function of temperature. Despite all these difficulties, some qualitative information can be extracted from the spectra obtained in the low-temperature domain (slow motion limit where the interactions are not averaged) and in the high-temperature domain (fast motion limit where all the interactions are averaged).

Figure 4 shows experimental spectra recorded at 170 K (a), 290 K (b), 480 K (c), and 800 K (d). For each spectrum, the result of the fitting is presented, either in the insert, for a and b spectra, or under the spectrum, for c and d spectra. Below 350 K, the dipolar interaction is not sufficiently averaged, and therefore, it masks all the structures (the quadrupolar one and the structure due to the contributions of the different sites). From 170 to 200 K, only one broad Gaussian line accounts for the shape of the spectrum (Figure 4a). Above 200 K, two Gaussian/Lorentzian lines are needed (Figure 4b). The ratio of the contributions of the narrow line and the broad line is 39:61. This ratio is very close to the one expected for the two contributions of the central line and the satellites ones for a $I = {}^3/_2$ spin system, i.e., 40:60. As temperature increases above 350 K, the deconvolution of the experimental spectra becomes

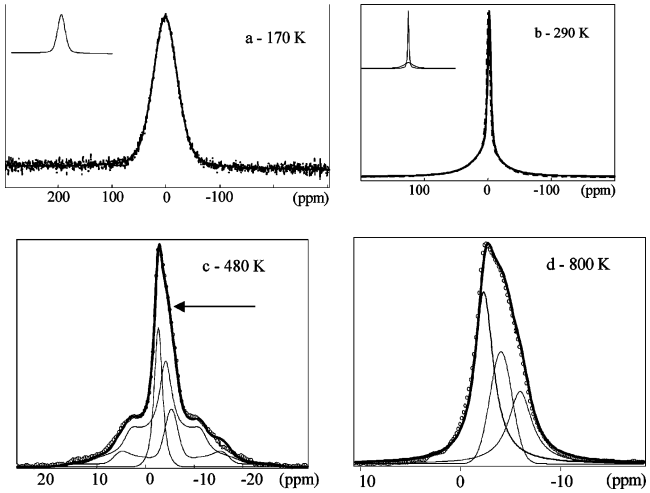


**Figure 4.** Static $^7Li$ NMR spectra recorded at 170 K (a), 290 K (b), 480 K (c), and 800 K (d) ($\nu_0 = 116$ MHz). Experimental line (dashed and dotted lines) and fitting lines (full lines)

complex and evolves with temperature. At 390 K, the quadrupolar structure begins to merge and the spectrum can be deconvoluted with a Gaussian line ($\approx 25\%$) and a quadrupolar line ($\approx 75\%$). Above this temperature, the deconvolution is more complex. This may be due to one or several reasons invoked previously. Nevertheless, some attempts have been made to propose a spectral deconvolution. For 390 K $< T <$ 500 K, when the satellites are observed (Figure 4c), the spectra, which are not symmetric (the arrow indicates a slope change), can be fitted with a minimum of three lines: one Gaussian/Lorentzian line and two quadrupolar ones in the ratio 20:20:60, respectively. As observed in Figure 4c, the fitting is not perfect, and certainly, the two quadrupolar contributions might be replaced by several more contributions and may be by a continuous distribution of quadrupolar lines. For higher temperatures ($T > 700$ K), when all the interactions are averaged and the quadrupolar structure is no longer observed (Figure 4d), the spectra can also be fitted with a minimum of three lines, three Gaussian/Lorentzian lines in the ratio 20:20:60. These three contributions can be distinguished despite the weak sensitivity to the chemical shift and the weak quadrupolar constant of the $^7Li$ nucleus. These contributions cannot be separated at low temperature, owing to the dipolar broadening; this explains the shape of the spectra recorded below 350 K. This line shape is specific to the niobate and has never been observed in the titanates.

MAS experiments have been performed, at the spinning frequency $\nu_r = 25$ kHz at room temperature, to provide support for our deconvolution model. We found three contributions at this temperature, but no more information concerning the relaxation times can be obtained because the lines are not separated despite the high spinning frequency used that narrows the lines.

These observations are consistent with the existence of several $Li^+$ sites with slightly different environments in the structure. The existence of several lines, even at high temperature, indicates, without doubt, that the assumption of $Li^+$ disorder can be ruled out. Indeed, such a disorder should be averaged at high temperature and should lead to spectra with only one line. On the other hand, this means that there are different $Li^+$ sites and that the $Li^+$ motion occurs between sites of the same kind (no exchange), even at high temperature. As temperature increases, the analysis of the spectra shows that the motion of the nucleus averages first the dipolar interaction, the central line considerably narrows, but the satellites can be observed.

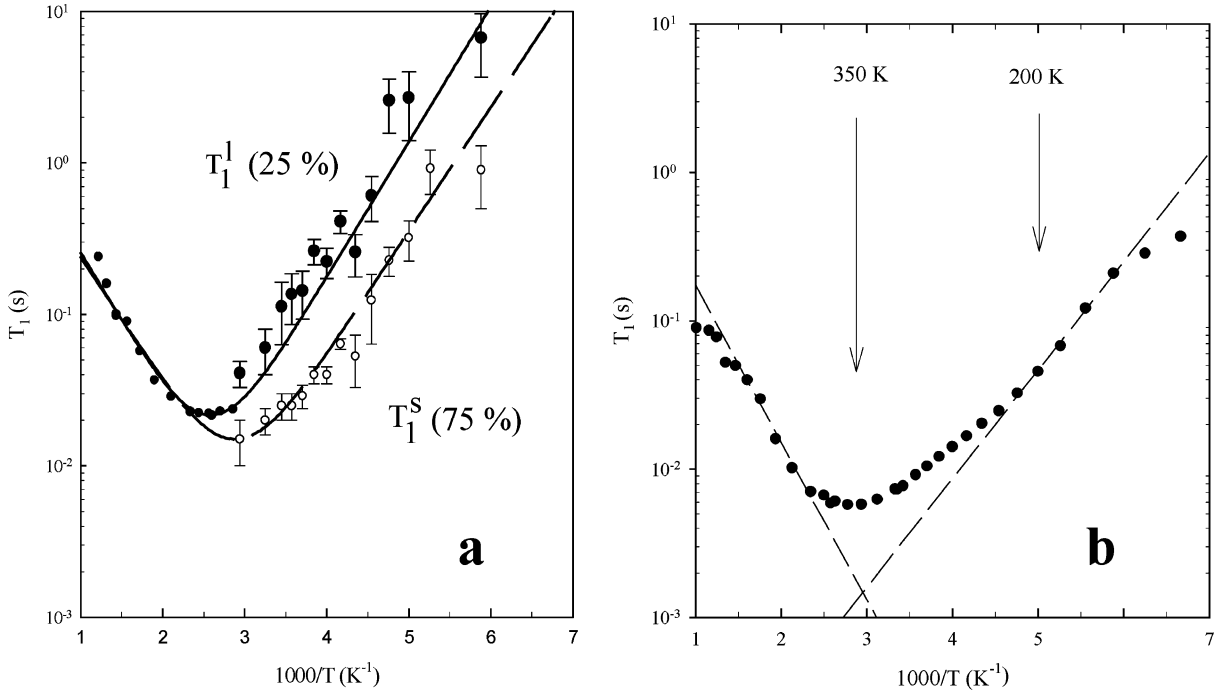


**Figure 5.** Logarithmic plots of the spin−lattice relaxation times, $T_1$, for $^7$Li ($\nu_0 = 116$ MHz) as a function of the inverse of temperature for (a) $Li_{3x}La_{1/3-x}NbO_3$ ($x = 0.04$) ((●) = $T_1^l$ and (○) = $T_1^s$), the full lines correspond to the $T_1$'s calculated from the BPP model, and (b) $Li_{3x}La_{2/3-x}TiO_3$ ($x = 0.11$) from ref 6.

Afterward, at higher temperature ($T > 700$ K), the spectrum does not exhibit any quadrupolar structure, the fast motion of the nucleus averages the quadrupolar interaction, and the static value of $\nu_Q$ decreases and sets to 0. This leads to the progressive transformation of the quadrupolar lines into Gaussian/Lorentzian ones, as shown in Figure 4c and d.

The Gaussian/Lorentzian line, that contributes around 20% of the spectrum and that appears whatever the temperature is, can be assigned to $Li^+$ ions in an isotropic environment with no distortion and then no field gradient. On the other hand, the quadrupolar lines, that contributes around 80% of the spectrum, can be assigned to $Li^+$ ions in distorted environments with a small but a non-negligible field gradient, i.e., $\nu_Q \neq 0$. Because the quadrupolar constant is small ($\nu_Q < 2$ kHz at 480 K), the distortions should be weak, although the $^7$Li quadrupolar moment is small. The presence of distortions in the A-cages of the oxide is related, without doubt, to the environment of this A-cage, i.e., to the nature of the first ($O^{2-}$), the second ($Nb^{5+}$), and/or the third neighbors ($La^{3+}$, $Li^+$, vacancies) of $Li^+$ nucleus. Owing to both the thermal agitation and the dynamics of the $Li^+$ ions, these distortions vary with temperature and disappear as temperature increases. In the titanates $Li_{3x}La_{2/3-x}TiO_3$, the same features have been observed, except that we have shown that all the sites are weakly distorted.[6−9]

**$^7$Li NMR Spin−Lattice Relaxation Times.** The continuous broadening of the central line, observed in Figure 3 as temperature decreases, suggests that the quadrupolar interaction is not at the origin of the relaxation process. Indeed, in the case of quadrupolar fluctuations, there is no adiabatic broadening contribution to the homogeneous linewidth of the central transition, and at low temperature (in the slow motion regime), the linewidth of the central line would then be only due to the lifetime of the energy level, and consequently, the linewidth should become constant. This is not observed in our experiments, and therefore, we can assume that the broadening arises from the dipolar interaction. To confirm this assumption, $T_1$ experiments were performed on both $^7$Li and $^6$Li nuclei. The nuclear spin of this latter isotope is $I = 1$, and its quadrupolar moment is 60 times lower than that of the $^7$Li (i.e., $Q(^6Li) = -8 \times 10^{-32}$ m$^2$, $Q(^7Li) = -4.5 \times 10^{-30}$ m$^2$). If the relaxation mechanism is quadrupolar in nature, this would lead to a $T_1$ value for $^6$Li 3600 times greater than the $T_1$ value for $^7$Li. Experimentally, at room temperature, we found $T_1(^7Li) = 20$ ms and $T_1(^6Li) = 30$ ms. The ratio $T_1(^6Li)/T_1(^7Li) = 1.5$ is in the range of the squared ratio between the gyromagnetic constants of the two nuclei ($\approx 7$) (the difference may arise from the contributions of the spectral density at the different frequency measurements). Once again, this result clearly shows that the Li relaxation mechanism is not dominated by quadrupolar interaction. Thus, it is reasonable to assume that dipolar nuclear interaction is responsible for the Li relaxation in niobate, as is the case for the titanate.[4] Although the $^{17}$O are the first neighbors of $^7$Li, the $^7$Li−$^{17}$O dipolar interaction cannot be taken into account, owing to the very small natural abundance of $^{17}$O (i.e., $3.7 \times 10^{-2}$ %). Therefore, the dipolar coupling that governs the longitudinal relaxation must involve the second ($^{93}$Nb) or third ($^{139}$La, $^7$Li) next-nearest neighbors of $^7$Li. The dipolar relaxation due to paramagnetic impurities could also be invoked. However, EPR measurements performed at room temperature do not evidence the presence of such impurities.

Figure 5a shows the variation of the spin−lattice relaxation time $T_1$ of $^7$Li nucleus as a function of the inverse of temperature for $Li_{3x}La_{1/3-x}NbO_3$ ($x = 0.04$) in the temperature range from 150 to 900 K. For comparison, Figure 5b presents the same plot for the titanate according to ref 4. The $T_1$ curve for the niobate displays a totally different behavior than the one observed for the titanate. For the niobate, at low temperatures (slow motion), two values of $T_1$ are evidenced and only one is observed at high temperature (fast motion), for $T > 500$ K. For the titanate, only one $T_1$ is observed whatever the temperature is. The $T_1$ values have been obtained from the experimental magnetization vs time curves that are slightly different for both compounds, as shown in Figure 6. For the niobate, when $T >$ RT, the magnetization *vs* time curves follow a monoexponential

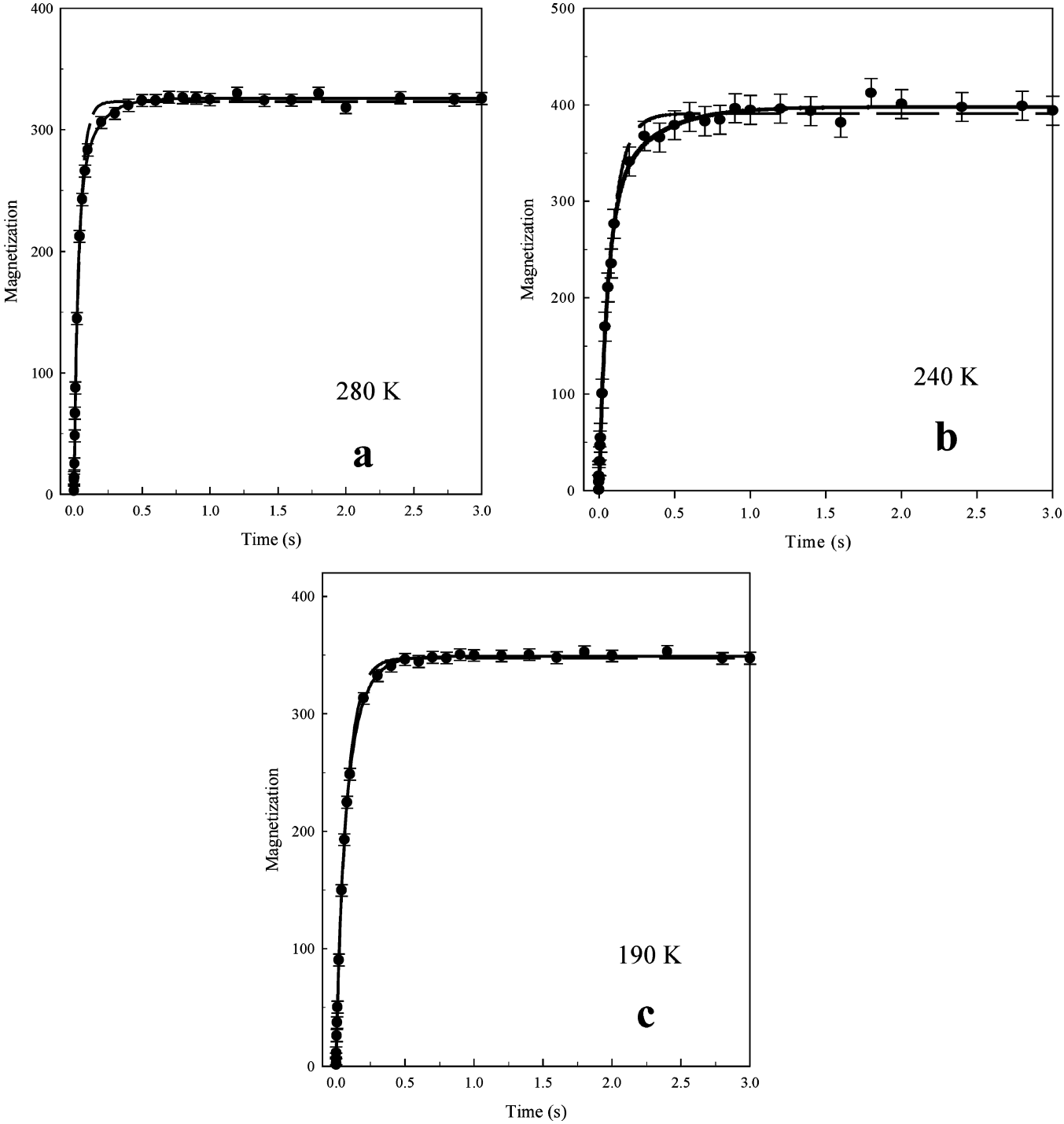


**Figure 6.** Magnetization curves for $^7$Li ($\nu_0 = 116$ MHz) recorded (a) at 280 K, (b) at 240 K for $Li_{3x}La_{1/3-x}NbO_3$ ($x = 0.04$), and (c) at 190 K for $Li_{3x}La_{2/3-x}TiO_3$ ($x = 0.11$). Dots refer to the experimental data, dashed line to the fitting with only one relaxation time (relationship 1), and full line refers to the fitting with two relaxation times (relationship 2).

behavior and the curves are well fitted according to the relationship (eq 1). On the other hand, below room temperature, the magnetization vs time curves follow a two-exponential behavior corresponding to two values of $T_1$ (Figure 6a and b). The relationship in eq 2 is then used for the fitting. In Figure 6, dots refer to the experimental data, the dashed line refers to the calculated curve with only one $T_1$ (relationship (eq 1)), and the full line to the calculated curve with two $T_1$ (relationship (eq 2)). The presence of two $T_1$ leads to the particular curvature of the magnetization vs time curve in the time range from 200 to 1000 ms. This curvature increases as temperature decreases. It is worth noting that the existence of two values of $T_1$ has been observed in the layered tantalates,[28] but it has never been observed in LLTO titanates, as shown in Figure 6c. In these latter compounds, the curves are perfectly fitted by using the relationship (eq 1) in the whole temperature range investigated, i.e., 150−900 K.

Below 500 K, two $T_1$ are observed, $T_1^s$ and $T_1^l$. $T_1^s$ is related to a short relaxation time (s); it contributes to around 75% to the total magnetization. $T_1^l$ is related to a long relaxation time (l); its contribution to the total magnetization is only 25%. Owing to these contributions, the presence of the two $T_1$ values cannot be ascribed to the quadrupolar nature of the nucleus spin ($I = 3/2$) of the $^7$Li. According to refs 22−27, a $I = 3/2$ nucleus leads theoretically in the slow regime to two $T_1$, one related to

a short relaxation time and a fast process ($T_1^s$), with a contribution of 20%, and a second one, related to a long relaxation time and a slow relaxation process ($T_1^l$), with a contribution of 80%. Such contributions are not observed in this niobate. However, the values of 25% for $T_1^l$ and 75% for $T_1^s$ are close to the contributions of the Gaussian/Lorentzian line ($\approx$ 20%) and of the several quadrupolar lines ($\approx$ 80%), previously reported in the spectrum analysis. Therefore, the two curves in Figure 5a can be assigned to the longitudinal relaxation of the two kinds of $Li^+$ ions present in the structure, the $Li^+$ ions in an isotropic environment (responsible of the Gaussian/Lorentzian line and of the $T_1^l$), and the $Li^+$ ions in distorted environments (responsible of the quadrupolar contributions and of the $T_1^s$). The results concerning $T_{1\rho}$ and $T_2$ will confirm this choice. It is worth noting that, in the titanate, into which two different $Li^+$ ions are detected in the spectra, all residing in weakly distorted environments, only one $T_1$ is measured.

Each $T_1$ vs 1000/$T$ curve of Figure 5a displays a minimum, one at 385 K ($T_1^l$) and another one at 340 K ($T_1^s$). Both minima indicate a fluctuation correlation time of $\tau_c \approx 10^{-9}$ s around the room temperature for the two kinds of $Li^+$ ions. Such small correlation times are linked to a fast motion of the $Li^+$ ions. As for the titanates, it can be postulated that this motion corresponds to the localized motion of the mobile ion inside the A-cage of the perovskite structure.

According to the Bloemberger−Purcell−Pound (BPP) model,[29] which assumes an isotropic motion of particles (3D motion) and a pure exponential correlation function, each $T_1$, ($T_1^l$), and ($T_1^s$) must follow the relationship (eq 5):

$$\frac{1}{T_1^i} = C_i\left(\frac{\tau_c^i}{1+(\omega_0\tau_c^i)^2} + \frac{4\tau_c^i}{1+(2\omega_0\tau_c^i)^2}\right) \qquad (5)$$

where $i$ stands for "s" or "l", $\omega_0 = 2\pi\nu_0$ ($\nu_0 = 116$ MHz, the Larmor Frequency for $^7$Li with our equipment). For each relaxation, the $C$ value is determined from the minimum of the $T_1$ vs 1000/$T$ curve, shown in Figure 5a, where $\omega_0\tau_c = 0.62$. The activation energy, $E_a = 0.17 \pm 0.02$ eV, is determined from the high-temperature part of $T_1$. The correlation times of the motions are thermally activated and follows the well-known Arrhenius law:

$$\tau_c = \tau_c^0 \exp\frac{E_a}{RT} \qquad (6)$$

The correlation time of the relaxation, corresponding to the long relaxation time, $T_1^l$, is characterized by a prefactor $\tau_c^0 = (4.3 \pm 0.1) \times 10^{-12}$ s. The correlation time of the relaxation corresponding to the short relaxation time, $T_1^s$, is characterized by a slightly smaller prefactor $\tau_c^0 = (3.8 \pm 0.1) \times 10^{-12}$ s. These values of $\tau_c^0$ corresponds to an attempted frequency on the order of $\nu^0 \approx 4 \times 10^{10}$ Hz. This frequency is 2 orders of magnitude lower than the lattice frequency. This result is not yet understood and remains to be explained. The lines in Figure 5a represent the $T_1$ values calculated in the whole temperature range investigated from 150 to 900 K according to the BPP model (relationship (eq 5)) with C, $E_a$, and $\tau_c^0$, as previously determined. It can be observed that $T_1^s$ follows the BPP model in the whole temperature range. This result suggests that the fast relaxation process proceeds in a 3D dimension. On the other hand, the experimental $T_1^l$, at low temperature, are slightly higher than the values expected from the BPP model, suggesting that the slow relaxation process, probed by $T_1^l$, may not be a three-dimensional one. However, owing to the experimental errors in the determination of the values of $T_1$, much care has to be taken in this conclusion, and further experiments, such as relaxometry, are necessary to study the assumed change of dimensionality of the $Li^+$ ions motion in the symmetric sites.

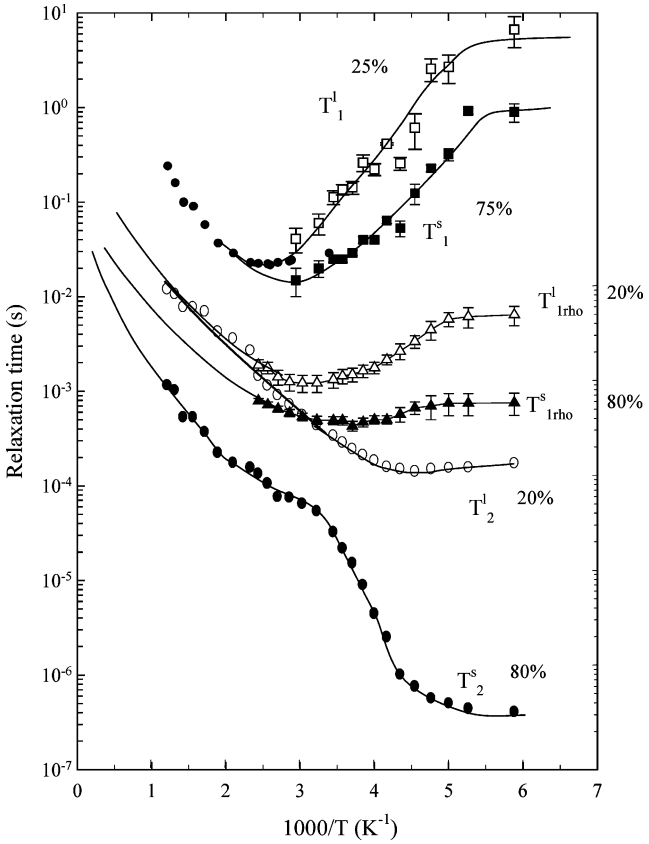


**Figure 7.** Logarithmic plots of $T_1$ (□), $T_{1\rho}$ (△), and $T_2$ (○) for $^7$Li as a function of temperature for $Li_{3x}La_{1/3-x}NbO_3$ ($x = 0.04$). The white symbols represent the long relaxation times and the black ones the short relaxation times (the full lines are only guide for the eyes).

The above results show that the localized motion of the $Li^+$ ions in the A-site of the perovskite structure is slightly different according to the environment of the A-cage. The $Li^+$ ions that reside in A-cages with high symmetry ($\approx$ 20%) undergo a slow relaxation process, probed by the long relaxation time $T_1^l$; they are responsible for the Gaussian/Lorentzian line shape in the spectra. The $Li^+$ ions that reside in distorted A-cages ($\approx$ 80%) undergo a slightly faster relaxation process, probed by the short relaxation time $T_1^s$, with a quadrupolar line shape. Furthermore, it seems that the dimension of the motion is not identical for all the $Li^+$ ions of the niobate (in the limit of the experimental accuracy).

Figure 7 shows the variation of the relaxation times $T_1$, $T_{1\rho}$, and $T_2$ of the $^7$Li nucleus as a function of the inverse of temperature for $Li_{3x}La_{1/3-x}NbO_3$ ($x = 0.04$). A very important feature is shown in this figure: at low temperature, there are two contributions (around 20−80%) for each relaxation time. Furthermore, these curves clearly evidence (i) the existence of two motions of the $Li^+$ ions and (ii) the existence of different $Li^+$ sites, as previously discussed; this shows that these different $Li^+$ ions can be also differentiated by their dynamics.

Two particular features of these curves evidence the existence of two different motions of $Li^+$ ions: first, the presence of the two minima in $T_1$ and $T_{1\rho}$ curves, and second, the fact that the $T_{1\rho}$ and $T_2$ curves do not join the $T_1$ curve at high temperature, as would be the case if these three relaxation times probe the

same motion. The two $T_{1\rho}$ curves exhibit minima at 310 K for the long relaxation time, $T^{l}_{1\rho}$, and at 265 K for the short one, $T^{s}_{1\rho}$. These minima indicate a fluctuation correlation time of $\tau_c \approx 10^{-6}$ s (according to the relationship at the minimum $\omega_1\tau_c = 0.62$, with $\omega_1 = 2\pi\nu_1$). These two last temperatures are not really different from the temperatures of the minima of the two relaxation times, $T^{l}_{1}$ and $T^{s}_{1}$, and cannot account for the difference of the 3 orders of magnitude of the correlation times $\tau_c$ with the small activation energy (0.17 eV measured in high temperature or fast regime). Therefore, the correlation time of $\tau_c \approx 10^{-6}$ s, measured around 300 K and probed by $T_{1\rho}$, has to be associated, without doubt, to another motion than the fast motion probed by $T_1$ and related to a correlation time of $\tau_c \approx 10^{-9}$ s. The correlation time of $\approx 10^{-6}$ s must then be related to a slow motion of the $Li^+$ ions. The second feature that indicates the presence of two motions is the fact that, at high temperature, $T_{1\rho}$ and $T_2$ curves do not join the $T_1$ one, whereas they tend to meet, as shown by the lines drawn in the curves. These results imply also that $T_{1\rho}$ and $T_2$ probe a slow motion and $T_1$ a fast one. As for the titanates, it can be postulated that this slow motion corresponds to the hopping of the $Li^+$ ions from one A-cage to a next vacant A-cage of the perovskite structure. This motion gives rise to the dc conductivity measured in the niobates. The fast motion, probed by $T_1$, corresponds to the localized motion of the mobile ion inside the A-cage of the perovskite structure, as discussed previously. The slow motion will have some effect on the $T_1$ at high temperature when the $T_1$ of the fast motion will be so long that it can no longer relax the $^7$Li nucleus. Such an effect is observed in the titanates around 1000 K when saturation of the $T_1$ occurs (Figure 5b).

The existence of different $Li^+$ sites is also evidenced by the presence of two $T_1$, two $T_{1\rho}$, and two $T_2$. The contributions of the long relaxation times (l) and of the short relaxation times (s) are always around 20% and 80%, respectively. As for $T_1$, the presence of two $T_{1\rho}$ and two $T_2$ values with the above-reported contributions cannot be ascribed to the quadrupolar nature of the nucleus spin ($I = {}^3/_2$) of the $^7$Li. Therefore, they can be ascribed to two types of $Li^+$ ions present in the oxide.

It is worth noting that, as concluded from the analysis of the spectra, the $Li^+$ of these sites do not exchange at high temperature because the two sets (20% and 80%) of $T_{1\rho}$ and $T_2$ curves do not tend to join at high temperature. These two contributions are ascribed, for the smallest one, to $Li^+$ ions in the isotropic environment; these ions are responsible for the Gaussian/Lorentzian line of the spectra, the $T^{l}_{1}$, the $T^{l}_{1\rho}$, and $T^{l}_{2}$, and for the more important one, to $Li^+$ ions in distorted environments, which are responsible for the quadrupolar contributions, the $T^{s}_{1}$, the $T^{s}_{1\rho}$, and the $T^{s}_{2}$, respectively. The occurrence of only one $T_1$ at high temperature is not contradictory to the existence of two $Li^+$ sites. It means that these $Li^+$ sites cannot be differentiated by their fast motion, which is attributed to their motion inside the A-cages. On the other hand, they can be differentiated by their slow motion from A-cage to A-cage, as reported by $T_{1\rho}$ and $T_2$. This has been already found in the titanates. The most important difference between the niobate and the titanate lies in the behavior in the fast regime, where two sets of $T_{1\rho}$ and $T_2$ remain in the niobates, whereas only one is evidenced in LLTO.[4] This means that exchange occurs between the different $Li^+$ in LLTO, whereas they do not exchange in the niobates. The crystallographic structure and, mostly, the different $La^{3+}$ distribution in the A-cages of the double-cell perovskites can be responsible for this behavior. The above discussion is confirmed by the two rigid lattice limits of $T_2$. This regime is attained at higher temperature for $Li^+$ ions in the most symmetric environment than for $Li^+$ ions in the distorted ones. This also suggests a stronger coupling of the former ions to the lattice and then a different environment of the mobile ion.

## Conclusion

The total substitution of $Nb^{5+}$ for $Ti^{4+}$ in the perovskite $Li_{3x}La_{2/3-x}TiO_3$ leads to a change in the $La^{3+}$ ions distribution in the A-sites of the double-cell perovskite structure of the niobate. A $La^{3+}$-rich layer, which is occupied at around 55% by $La^{3+}$ ions, and a $La^{3+}$-poor layer, which can be considered as empty, are determined by XRD patterns refinement. The nature and the valence of the metal transition as well as the distribution of $La^{3+}$ ions give rise to different A-cages into which the $Li^+$ ions reside between hopping. Some are more symmetric than others. This leads to $Li^+$ ions with slightly different environments. Because these different ions do not exchange, even at high temperature, they can be differentiated in $^7$Li NMR spectra. The Gaussian/Lorentzian line that contributes around 20% of the spectrum and that appears whatever the temperature can be assigned to $Li^+$ ions in an isotropic environment with no distortion and then no field gradient. On the other hand, the quadrupolar lines that contribute around 80% of the spectrum can be assigned to $Li^+$ ions in distorted environments with a small but a non-negligible field gradient. This ratio, 20:80, is also found in the $T_1$ (at low temperature), $T_{1\rho}$, and $T_2$ (whatever the temperature) relaxation time contributions.

As for LLTO, $T_1$ and $T_{1\rho}$ probe two different motions. The fast motion, probed by $T_1$, corresponds to the localized motion of $Li^+$ inside the A-cage of the perovskite structure, and the slow motion, probed by $T_{1\rho}$, corresponds to the hopping of the $Li^+$ ions from one A-cage to the next vacant one. However, important differences between the niobate and LLTO are observed in the behavior of the $Li^+$ dynamics. The relaxation time curves show that, in the niobate, the fast motion of the two types of $Li^+$ ions behaves similarly at high temperature (only one $T_1$), whereas their slow motion remains different whatever the temperature is (two $T_{1\rho}$ and two $T_2$), confirming that these $Li^+$ ions do not exchange, even at high temperature. Finally, $^7$Li and $^6$Li $T_1$ values show that the Li relaxation mechanism is not dominated by quadrupolar interaction.

## References and Notes

(1) Belous, A. G.; Novitskaya, G. N.; Polyanetskaya, S. V.; Gornikov, Yu. I. *Russ. J. Inorg. Chem.* **1987**, *32*, 156.

(2) Inaguma, Y.; Chen, L.; Itoh, M.; Nakamura, T.; Uchida, T.; Ikuta, H.; Wakihara, M. *Solid State Commun.* **1993**, *86*, 689.

(3) Inaguma, Y.; Chen, L.; Itoh, M.; Nakamura, T. *Solid State Ionics* **1994**, *70/71*, 196.

(4) Emery, J.; Bohnké, O.; Fourquet, J.-L.; Buzaré, J.-Y.; Florian, P.; Massiot, D. *J. Phys.: Condens. Matter* **2002**, *14*, 523.

(5) Bohnké, O.; Emery, J.; Veron, A.; Fourquet, J.-L.; Buzaré, J.-Y.; Florian, P.; Massiot, D. *Solid State Ionics* **1998**, *109*, 25.

(6) Bohnké, O.; Badot, J.-C.; Emery, J. *J. Phys.: Condens. Matter* **2003**, *15*, 7571.

(7) Fourquet, J.-L.; Duroy, H.; Crosnier-Lopez, M.-P. *J. Solid State Chem.* **1996**, *127*, 283.

(8) Inaguma, Y.; Katsumata, T.; Itoh, M.; Morii, Y. *J. Solid State Chem.* **2002**, *166*, 67.

(9) Bohnké, O.; Bohnké, C.; Fourquet, J.-L. *Solid State Ionics* **1996**, *91*, 21.

(10) Bohnké, O.; Emery, J.; Fourquet, J.-L. *Solid State Ionics* **2003**, *158*, 119.

(11) Bohnké, O.; Emery, J.; Fourquet, J.-L.; Badot, J.-C. *Recent Res. Dev. Solid State Ionics* **2003**, *1*, 47−86.

(12) Belous, A. G. *Solid State Ionics* **1996**, *90*, 193.

(13) Belous, A. G. *Ionics* **1997**, *3*, 117.

(14) Belous, A. G.; Gavrilenko, O. N.; Pashkova, E. V.; Mirnyi, V. N. *Russ. J. Electrochem.* **2002**, *38*, 425.
(15) Belous, A.; Pashkova, E.; Gavrilenko, O.; V'yunov, O.; Kovalenko, L. *J. Eur. Ceram. Soc.* **2004**, *24*, 1301.
(16) Kawakami, Y.; Ikuta, H.; Wakihara, M. *J. Solid State Electrochem.* **1998**, *2*, 206.
(17) Garcia-Martin, S.; Rojo, J. M.; Tsukamoto, H.; Moran, E.; Alario-Franco, M. A. *Solid State Ionics* **1999**, *116*, 11.
(18) Garcia-Martin, S.; Alario-Franco, M. A. *J. Solid State Chem.* **1999**, *148*, 93.
(19) Latie, L.; Villeneuve, G.; Conte, D.; LeFlem, G. *J. Solid State Chem.* **1984**, *51*, 293.
(20) Rodriguez Carjaval, J. *FULLPROF Program: Rietveld Pattern Matching Analysis of Powder Patterns*; ILL: Grenoble, 1990.
(21) Massiot, D.; Thiele, H.; Germanius, A. Bruker Report No. 43, 1994; p 140.
(22) Delville, A.; Porion, P.; Faugère, A. M. *J. Phys. Chem. B* **2000**, *104*, 1546.
(23) Petit, D.; Korb, J. P. *Phys. Rev. B* **1988**, *37*, 5761.
(24) McLachlan, A. D. *Proc. R. Soc. London* **1964**, *A280*, 271.
(25) Hubbard, P. S. *J. Chem. Phys.* **1970**, *53*, 985.
(26) Bull, T. E. *J. Magn. Res.* **1972**, *8*, 344.
(27) Werbelow, L. G. *J. Chem. Phys.* **1979**, *70*, 5381.
(28) Le Berre, F.; Crosnier-Lopez, M.-P.; Laligant, Y.; Suard, E.; Bohnké, O.; Emery, J.; Fourquet, J.-L. *J. Mater. Chem.* **2004**, *14*, 3548.
(29) Bloembergen N.; Purcell, E. M.; Pound, R. V. *Phys. Rev.* **1948**, *73*, 679.